

# Realization of an Electrically Tunable Narrow-Bandwidth Atomically Thin Mirror Using Monolayer MoSe<sub>2</sub>

**Review Article****Author(s):**

Back, Patrick; Zeytinoglu, Sina; Ijaz, Aroosa; Kroner, Martin; Imamoglu, Atac

**Publication date:**

2018-01-18

**Permanent link:**

<https://doi.org/10.3929/ethz-b-000231337>

**Rights / license:**

[In Copyright - Non-Commercial Use Permitted](#)

**Originally published in:**


Physical Review Letters 120(3), <https://doi.org/10.1103/physrevlett.120.037401>

**Funding acknowledgement:**

676108 - Nanoscale solid-state spin systems in emerging quantum technologies (EC)  
671000 - Interacting polaritons in two-dimensional electron systems (EC)

# Realization of an Electrically Tunable Narrow-Bandwidth Atomically Thin Mirror Using Monolayer MoSe<sub>2</sub>

Patrick Back, Sina Zeytinoglu, Aroosa Ijaz, Martin Kroner, and Atac Imamoğlu  
*Institute for Quantum Electronics, ETH Zürich, CH-8093 Zurich, Switzerland*

 (Received 12 July 2017; revised manuscript received 21 November 2017; published 18 January 2018)

The advent of two-dimensional semiconductors, such as van der Waals heterostructures, propels new research directions in condensed matter physics and enables development of novel devices with unique functionalities. Here, we show experimentally that a monolayer of MoSe<sub>2</sub> embedded in a charge controlled heterostructure can be used to realize an electrically tunable atomically thin mirror, which effects 87% extinction of an incident field that is resonant with its exciton transition. The corresponding maximum reflection coefficient of 41% is only limited by the ratio of the radiative decay rate to the nonradiative linewidth of exciton transition and is independent of incident light intensity up to 400 W/cm<sup>2</sup>. We demonstrate that the reflectivity of the mirror can be drastically modified by applying a gate voltage that modifies the monolayer charge density. Our findings could find applications ranging from fast programable spatial light modulators to suspended ultralight mirrors for optomechanical devices.

DOI: [10.1103/PhysRevLett.120.037401](https://doi.org/10.1103/PhysRevLett.120.037401)

A plethora of groundbreaking experiments have established monolayers of transition metal dichalcogenides (TMDs), such as MoSe<sub>2</sub> or WSe<sub>2</sub>, as a new class of two-dimensional direct band-gap semiconductors [1–5]. In the absence of free carriers, the lowest energy elementary optical excitations in TMDs are excitons with an ultralarge binding energy of  $\sim 0.5$  eV [6]. Encapsulation of TMD monolayers with hexagonal boron nitride (*h*-BN) [7,8] dramatically improves the optical quality, yielding an exciton linewidth  $\sim 2$  meV [9,10]. These narrow linewidths have a dominant contribution from radiative decay of  $\sim 1.5$  meV for MoSe<sub>2</sub> [11,12]. Motivated by these developments, we previously analyzed the optical response of a monolayer TMD theoretically [13] and showed that it realizes an atomically thin mirror [13–15].

Here, we present experiments demonstrating that a *h*-BN encapsulated MoSe<sub>2</sub> monolayer has a reflectivity exceeding 40% and an extinction of resonant transmitted light approaching 90%. Figure 1(a) shows a micrograph of the charge tunable heterostructure we have studied: a 9 by 4  $\mu\text{m}$  MoSe<sub>2</sub> monolayer is sandwiched between two *h*-BN layers. The heterostructure is placed on top of a transparent fused-silica substrate and capped with bilayer graphene. A gate voltage  $V_g$  applied between bilayer graphene and the MoSe<sub>2</sub> layer allows for tuning the electron density  $n_e$  [16,17], thereby modifying the resonance frequency as well as the nature of the elementary optical excitations [12].

To the extent that the MoSe<sub>2</sub> monolayer and its environment is homogeneous, in-plane momentum  $k$  is a good quantum number for both exciton and radiation field modes. We emphasize that in-plane translational invariance is an essential property of an ideal mirror. The quality of a realistic mirror can in turn be assessed by the ratio of

momentum conserving specular reflection to light that is absorbed (by inelastic processes) or scattered (by disorder) into other momentum states. The latter is given by  $1 - (R + T)$  where  $R$  and  $T$  are the specular reflection and transmission coefficients. In our experiments, this ratio is  $R/(1 - R - T) = 0.8$ . Unless otherwise stated, the terms “reflection” and “transmission” are used for momentum conserving processes only.

Figure 1(b) depicts the outline of our experiments where we use resonant light to probe excitonic excitations. The outgoing right-propagating electric field mode  $E_{\text{out}}^r(\omega)$  [Fig. 1(b)] can be expressed in terms of the incident field modes  $E_{\text{in}}^r(\omega)$  and  $E_{\text{in}}^l(\omega)$  [13]

$$E_{\text{out}}^r(\omega) = \frac{\Gamma/2}{\Gamma/2 - i(\omega - \omega_{\text{exc}})} [(1 - \eta)E_{\text{in}}^r(\omega) - \eta E_{\text{in}}^l(\omega)], \quad (1)$$

where  $\omega_{\text{exc}}$  and  $\Gamma$  denote the transition frequency and the radiative decay rate of the excitons.  $\eta = \Gamma/\gamma_{\text{tot}}$  gives the ratio of radiative decay rate to the total exciton line broadening  $\gamma_{\text{tot}}$ . Hence,  $\gamma_{\text{tot}} - \Gamma$  describes Lorentzian absorption processes such as the nonradiative recombination, as well as the nonspecular scattering processes induced by the disorder potential. In our experiments  $E_{\text{in}}^r(\omega) = E_{\text{inc}} \neq 0$ , whereas  $E_{\text{in}}^l(\omega) = 0$ ; in this limit, the reflected and transmitted fields are given by  $E_{\text{refl}} = E_{\text{out}}^l(\omega)$  and  $E_{\text{trans}} = E_{\text{out}}^r(\omega)$ , respectively. The minimum and maximum (resonant) intensity transmission and reflection coefficients are given by  $T_{\text{min}} = (\gamma_{\text{tot}} - \Gamma)^2/\gamma_{\text{tot}}^2$  and  $R_{\text{max}} = \Gamma^2/\gamma_{\text{tot}}^2$ . These simple expressions, however, do not take into account the effects of the dielectric environment (see Supplemental Material [18]).

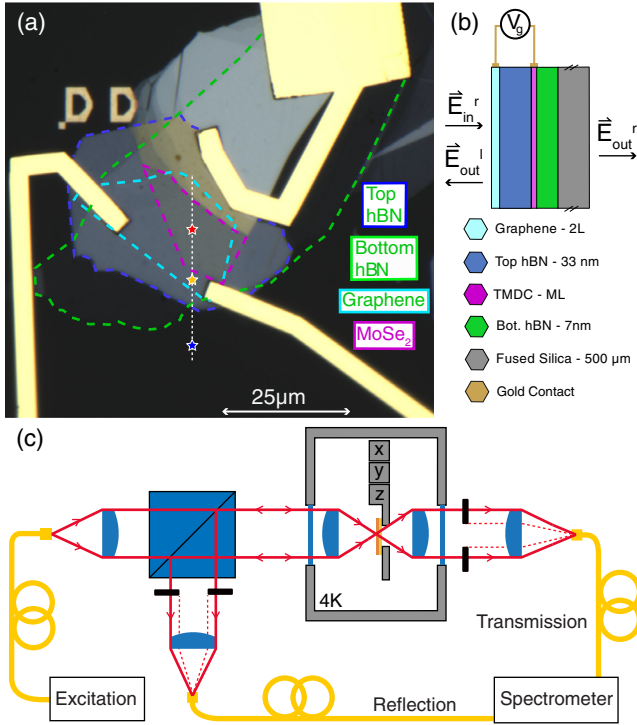


FIG. 1. (a) Micrograph of the measured heterostructure: the MoSe<sub>2</sub> monolayer is encapsulated in between 33 nm (top) and 7 nm (bottom) thick *h*-BN layers, which are indicated by blue and green dashed lines. The heterostructure is capped by a graphene bilayer and is placed on top of a transparent 500 μm thick fused-silica substrate. The graphene and the MoSe<sub>2</sub> are electrically contacted by titanium and gold electrodes. The white line and colored stars indicate the position of optical measurements on and off the MoSe<sub>2</sub> and the *h*-BN layers. (b) Interaction of an incident field with a MoSe<sub>2</sub> monolayer. Optical fields can be characterized as consisting of right propagating input  $E_{in}^r$  and right and left propagating output modes  $E_{out}^r$ ,  $E_{out}^l$  respectively. (c) The schematic of the experimental setup. The sample is mounted in a helium flow cryostat in confocal configuration. The sample can be moved *in situ* by piezostepper motors. A collimated excitation beam is focused onto the sample by the first lens. The reflected light is collimated again by the same lens (NA = 0.68). The transmitted light is collimated by the second lens (NA = 0.55). By reducing the diameter of the collection beam, we can reduce the effective NA of the detection optics.

We measure the transmission and reflection spectrum of the heterostructure in a cryogenic transmission microscope at  $T = 4$  K with free space optical access as shown in Fig. 1(c). The incident light is focused to a diffraction limited spot with diameter  $\approx 700$  nm, while the transmitted or reflected light is collected with very low numerical aperture (NA) in order to ensure that we predominantly measure specular reflection or transmission of light with in-plane momentum  $\approx 0$ . For the excitation, we use either a broadband light emitting diode centered at 780 nm or a tunable single-mode Ti:S laser. Because of losses on the windows of the cryostat and the finite coupling and

detection efficiency, we cannot directly measure the absolute reflected and transmitted power. Instead, we use a reference reflection and transmission spectrum of the incident light by moving our excitation spot off the MoSe<sub>2</sub> layer or off the heterostructure to the fused-silica layer.

Figure 2(a) shows the intensity reflection coefficient of light with a photon energy of 1.64 eV as we move the excitation or detection spot along the white line indicated in Fig. 1(a). In the region around the blue spot, we measure the reflectivity of the fused-silica layer; the extracted reflection coefficient of  $8 \pm 1\%$  (see Supplemental Material [18]) is in good agreement with the 9.57% reflection we would expect from a thick fused-silica layer. Moving to the orange spot, where we have the graphene/*h*-BN heterostructure without the MoSe<sub>2</sub> monolayer, we observe a sizeable increase in reflection coefficient to about  $28\% \pm 5\%$ . Finally, reflection of the full heterostructure around the red spot exhibits very large variations in reflection coefficient ranging from 10% to more than 60%, demonstrating the ultrastrong optical response of monolayer MoSe<sub>2</sub>. Spatial variations in exciton resonance frequency, most likely stemming from the disorder profile, result in the observed position-dependent reflection coefficient of incident photons at a fixed frequency.

Figure 2(b) shows the normalized transmission spectrum obtained at the red spot [Fig. 1(a)], using a detection path NA of  $\sim 0.1$ . Even though the strong extinction of resonant light is evident, the dispersive line shape of the transmission spectrum does not allow us to read  $T_{min}$  of the monolayer directly from the data. To extract the maximal extinction, we obtain a fit to the experimental data using a transfer matrix model (red curve), which takes into account the dielectric environment of the TMD layer. The fit yields an extinction  $1 - T_{min} \approx 0.87 \pm 0.17$  for the bare TMD monolayer. We emphasize that extinction factors of this magnitude were previously only reported for transmon qubits coupled to superconducting microwave waveguides [22].

The reflection spectrum corresponding to the transmission data obtained at the red spot is depicted in Fig. 2(c). The stronger asymmetry in reflection originates from an optical interference between two contributions with comparable magnitude—the excitonic emission and the incident light reflected from the heterostructure. The transfer matrix fit (red curve) yields a maximal reflection coefficient of  $R = 0.41 \pm 0.08$  for the bare MoSe<sub>2</sub> layer.

Remarkably, the sum of specular reflection and transmission  $R + T$ , normalized to the corresponding value in the region around the orange spot, yields a nearly symmetric but Gaussian dip at the exciton resonance energy [Fig. 2(d)]: the reduction of the total measured  $R + T$  on resonance is a consequence of disorder induced scattering into high  $k$  excitonic modes. We emphasize the role of spatial fluctuations by noting that the reduction of  $R + T$  on resonance cannot be reproduced with a convolution of the

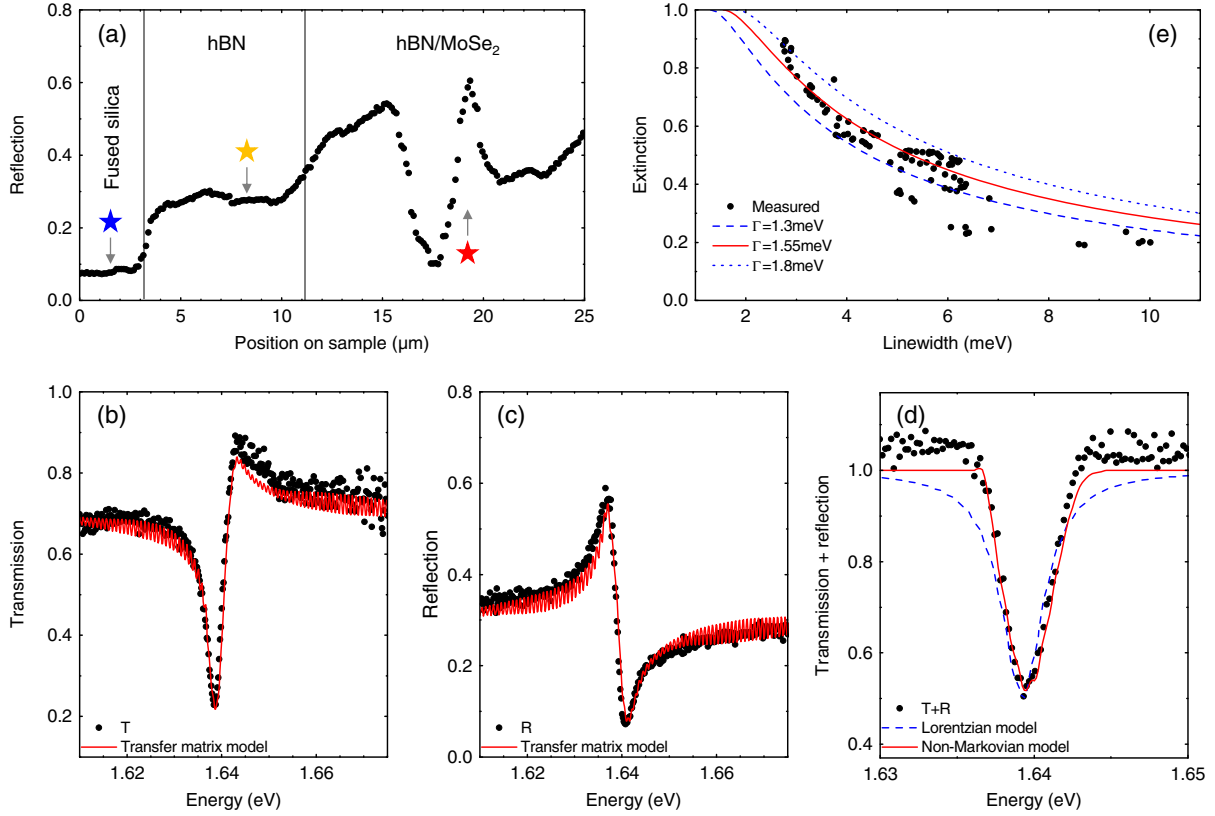


FIG. 2. (a) The measured reflection coefficient at a photon energy of 1.64 eV across the dashed white line indicated in Fig. 1(a). The reflection increases from 8% in the fused-silica region (blue star) to about 28% in the region having both top and bottom *h*-BN layers, as well as bilayer graphene (yellow star). The strong variations in reflection between 12 and 25  $\mu\text{m}$  stems from the position dependence of the exciton resonance of the MoSe<sub>2</sub>. The incident photons are resonant with the exciton transition at the position indicated by the red star. (b) Transmission as function of photon energy of the MoSe<sub>2</sub>/*h*-BN heterostructure measured at the position indicated by the red star with a detection arm numerical aperture of 0.1. The black dots represent the normalized data. The red line is a fit to experimental data obtained using transfer matrix formalism (see Supplemental Material [18]): small amplitude oscillations stem from Fabry-Perot effect associated with the silica substrate. (c) Reflection as function of photon energy measured under identical conditions as in (b). The transfer matrix calculations (red line) allows us to extract a resonant reflection enhancement by a factor of 1.46, indicating that the maximum reflectivity of a bare MoSe<sub>2</sub> monolayer is 41%. (d) Sum of the transmission and reflection spectra. Black dots represent the data, while the red line shows the transfer matrix calculations based on the same parameters used to obtain the fits to data shown in (b) and (c). The dashed blue line shows the best fit to reflection and transmission data obtained using a Markovian nonradiative decay rate. (e) Demonstration of linewidth dependence of maximal extinction. The black dots show the extracted extinction on resonance ( $1 - T_{\text{min}}$ ) as function of the measured linewidth  $\gamma_{\text{tot}}$  by fitting a dispersive Lorentzian model to the data. The lines indicate the dependence of the extinction as function of  $\gamma_{\text{tot}}$  for different radiative decay rates  $\Gamma$ .

radiatively broadened exciton peak with a Gaussian distribution of the excitonic transition frequencies due to purely temporal fluctuations. Indeed, such a description leads to  $R + T = 1$  for all detunings.

The strong deviation of the  $R + T$  spectrum from a Lorentzian unequivocally demonstrates the strongly non-Markovian nature of the disorder induced scattering processes. This feature stems from the dispersion of the  $k \neq 0$  excitons, which serve as a reservoir for  $k \approx 0$  excitons that we measure using our low NA detection. The resulting frequency dependent decay rate given by the imaginary part of the exciton self-energy  $\Sigma(\omega)$ , combined with transfer matrix calculations reproduces well the measured  $T$ ,  $R$ , as well as  $R + T$  data (see Supplemental Material [18]). We

remark that our findings, demonstrating that disorder induced scattering is the dominant nonradiative exciton line-broadening mechanism, is in agreement with four wave mixing experiments [23].

The aforementioned spatial inhomogeneity of the exciton resonance results in a variation of not only the exciton resonance energy, but also its linewidth across the sample for different locations of the excitation beam. Figure 2(e) shows the dependence of the extracted resonant coefficient on the linewidth of the exciton resonance, obtained by measuring transmission at different spots. We find that the broadened line shapes are reasonably well fit by dispersive Lorentzians, allowing us to compare the dependence of maximal extinction on total exciton linewidth  $\gamma_{\text{tot}}$  to the

theoretical value  $1 - (\gamma_{\text{tot}} - \Gamma)^2 / \gamma_{\text{tot}}^2$ . This comparison in turn allows us to determine the radiative decay rate to be in the range  $1.3 < \Gamma < 1.8$  meV, which is in good agreement with the values previously determined from normal-mode splitting of exciton polaritons [11,12]. We remark that, at the locations yielding the highest observed extinction factor of  $\sim 0.9$ , we extract consistently higher values of  $\Gamma$ . Finally, we remark that we have carried out transmission experiments on other samples, revealing a very similar dependence of the extinction on the exciton linewidth (see Supplemental Material Fig. S7 [18]).

To explore the nonlinearity of the TMD monolayer, we tuned a single-mode Ti:S laser into resonance with the MoSe<sub>2</sub> exciton transition and monitored the dependence of extinction on the laser intensity. Supplemental Material Fig. S6 [18] shows that the extinction remains unchanged as we vary the incident intensity by 4 orders of magnitude from 0.5 to 400 W/cm<sup>2</sup>. Verification of the theoretically predicted unusual saturation characteristics of TMD mirrors is likely to require pulsed laser excitation [13].

Because of strong exciton-electron interactions, the nature of elementary optical excitations can be drastically modified by applying  $V_g$ , which modifies the free electron density ( $n_e$ ) in the TMD monolayer [12]. A typical  $V_g$ -dependent transmission spectrum is shown in Fig. S4 (see Supplemental Material [18]): as  $n_e$  is increased, a new attractive exciton-polaron resonance that is red detuned by 25 meV with respect to the bare exciton transition emerges. The abrupt blueshift and broadening of the exciton resonance for  $V_g > -2$  V, on the other hand, can be understood as the transition from a bare exciton into a repulsive-exciton-polaron resonance. The  $V_g$  dependence of the optical response of the MoSe<sub>2</sub> monolayer indicates that the atomically thin mirror can be electrically tuned.

Figure 3(a) shows the  $V_g$  dependence of the maximal extinction coefficient obtained at exciton or repulsive-polaron resonance. The increase of minimum transmission from  $\sim 20\%$  down to 90% is due to a combination of electron-exciton interaction induced line broadening and oscillator strength transfer to attractive polaron. If we instead focus on the response to incident photons at a specific energy, we find an even sharper drop in extinction from 0.6 down to 0.1 upon increasing  $V_g$  from  $-2$  to 0 V, demonstrating electrical control of an atomically thin mirror [Fig. 3(a) inset]. With low resistance Ohmic contacts to the MoSe<sub>2</sub> monolayer, it should be possible to exploit the strong  $V_g$  dependence of excitonic response to realize fast switching of mirror transmission and reflection, potentially on subnanosecond time scales [24].

Because of the aforementioned oscillator strength transfer, maximal extinction at the attractive-polaron resonance first increases to about 0.2 before decreasing due to line broadening [Fig. 3(b)]. Even though the optical response of the attractive polaron is relatively modest, its strong dependence on the valley polarization of electrons and

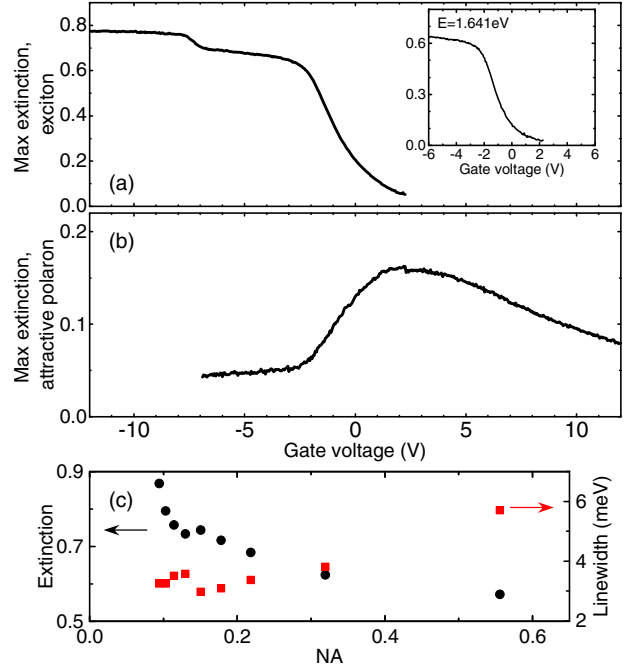


FIG. 3. (a) Gate voltage ( $V_g$ ) dependence of the maximal extinction of transmitted light using the exciton resonance. Injection of free carriers reduces the exciton oscillator strength and increases linewidth, leading to a sharp  $V_g$ -dependent drop in transmission. The inset shows the extinction of incident photons with a fixed energy of 1.641 eV as function of  $V_g$ , demonstrating that transmission can be changed from 10% to 60% by changing  $V_g$  by  $\sim 2$  V. (b)  $V_g$  dependence of maximal extinction at the attractive exciton-polaron resonance: the extinction increases with increasing electron density until  $V_g \sim 2$  V due to oscillator strength transfer from the exciton resonance. For  $V_g > 2$  V, excess line broadening suppresses the resonant enhancement of optical response. (c) Measured maximal extinction (black dots) and linewidth (red squares) as function of the NA of the detection optics. Increasing NA leads to an increase of the linewidth and a corresponding reduction of extinction. The observations are consistent with electron-hole exchange interaction induced splitting of  $s$ - and  $p$ -polarized excitonic resonances, which, in the absence of polarization selection, leads to line broadening.

its large  $g$  factor exceeding 15 [25] render it an excellent candidate for realization of chiral optical devices.

The experiments shown in Figs. 2(a)–2(d) as well as in Figs. 3(a) and 3(b) have been obtained by focusing the incident light onto a diffraction limited spot using a lens with NA = 0.68 and then collecting the transmitted or reflected light with a NA  $\sim 0.1$ . This allowed us to monitor the optical response of excitons with  $k \sim 0$ . Figure 3(c) shows the dependence of maximal extinction (black dots) and the corresponding linewidth (red squares) for several values of the transmission path NA, close to the same spot we used to obtain the data depicted in Fig. 2(b). We observe that, as we increase transmission NA from 0.1 to 0.55, the extinction drops from 0.9 down to 0.6, while the exciton linewidth increases from 3 to 6 meV. We tentatively

attribute this strong NA dependence to electron-hole exchange interaction induced modification of the exciton spectrum: it has been theoretically predicted that, due to this interaction, the  $p$ -polarized excitons would have a Dirac-conelike dispersion, leading to an energy splitting of  $s$ - and  $p$ -polarized excitons of order 3 meV for  $k \sim \omega_{exc}/c$  [26,27]. To the best of our knowledge, the NA-dependent increase in linewidth that we report here provides the first evidence for this striking theoretical prediction.

The strong optical response of a TMD monolayer as demonstrated in our experiments opens up new avenues for photonics. The combination of ultralight mass and strong optical response suggests that a suspended MoSe<sub>2</sub> monolayer could revolutionize the performance of optomechanical mass and force sensors. On the other hand, the possibility to drastically modify reflection on ultrashort time scales and subwavelength length scales using applied electric fields could open up new perspectives for digital mirror devices. Finally, the valley degree of freedom of exciton polarons can be used to realize chiral devices by introducing a ferromagnetic monolayer next to the optically active TMD layer [28].

This work is supported by a European Research Council (ERC) Advanced investigator grant (POLTDES) and Spin-NANO Marie Skłodowska-Curie Grant No. 676108.

- [1] B. Radisavljevic, A. Radenovic, J. Brivio, V. Giacometti, and A. Kis, *Nat. Nanotechnol.* **6**, 147 (2011).
- [2] A. Splendiani, L. Sun, Y. Zhang, T. Li, J. Kim, C.-Y. Chim, G. Galli, and F. Wang, *Nano Lett.* **10**, 1271 (2010).
- [3] B. W. H. Baugher, H. O. H. Churchill, Y. Yang, and P. Jarillo-Herrero, *Nat. Nanotechnol.* **9**, 262 (2014).
- [4] L. Britnell, R. M. Ribeiro, A. Eckmann, R. Jalil, B. D. Belle, A. Mishchenko, Y.-J. Kim, R. V. Gorbachev, T. Georgiou, S. V. Morozov, A. N. Grigorenko, A. K. Geim, C. Casiraghi, A. H. C. Neto, and K. S. Novoselov, *Science* **340**, 1311 (2013).
- [5] X. Xu, W. Yao, D. Xiao, and T. F. Heinz, *Nat. Phys.* **10**, 343 (2014).
- [6] A. Chernikov, T. C. Berkelbach, H. M. Hill, A. Rigosi, Y. Li, O. B. Aslan, D. R. Reichman, M. S. Hybertsen, and T. F. Heinz, *Phys. Rev. Lett.* **113**, 076802 (2014).
- [7] S. Latini, T. Olsen, and K. S. Thygesen, *Phys. Rev. B* **92**, 245123 (2015).
- [8] A. V. Stier, N. P. Wilson, G. Clark, X. Xu, and S. A. Crooker, *Nano Lett.* **16**, 7054 (2016).
- [9] O. A. Ajayi, J. V. Ardelean, G. D. Shepard, J. Wang, A. Antony, T. Taniguchi, K. Watanabe, T. F. Heinz, S. Strauf, X.-Y. Zhu, and J. C. Hone, *2D Mater.* **4**, 031011 (2017).
- [10] F. Cadiz, E. Courtade, C. Robert, G. Wang, Y. Shen, H. Cai, T. Taniguchi, K. Watanabe, H. Carrere, D. Lagarde, M. Manca, T. Amand, P. Renucci, S. Tongay, X. Marie, and B. Urbaszek, *Phys. Rev. X* **7**, 021026 (2017).
- [11] S. Dufferwiel, S. Schwarz, F. Withers, A. A. P. Trichet, F. Li, M. Sich, O. Del Pozo-Zamudio, C. Clark, A. Nalitov, D. D. Solnyshkov, G. Malpuech, K. S. Novoselov, J. M. Smith, M. S. Skolnick, D. N. Krizhanovskii, and A. I. Tartakovskii, *Nat. Commun.* **6**, 8579 (2015).
- [12] M. Sidler, P. Back, O. Cotlet, A. Srivastava, T. Fink, M. Kroner, E. Demler, and A. Imamoglu, *Nat. Phys.* **13**, 255 (2017).
- [13] S. Zeytinoglu, C. Roth, S. Huber, and A. Imamoglu, *Phys. Rev. A* **96**, 031801 (2017).
- [14] R. J. Bettles, S. A. Gardiner, and C. S. Adams, *Phys. Rev. Lett.* **116**, 103602 (2016).
- [15] E. Shahmoon, D. S. Wild, M. D. Lukin, and S. F. Yelin, *Phys. Rev. Lett.* **118**, 113601 (2017).
- [16] J. S. Ross, S. Wu, H. Yu, N. J. Ghimire, A. M. Jones, G. Aivazian, J. Yan, D. G. Mandrus, D. Xiao, W. Yao, and X. Xu, *Nat. Commun.* **4**, 1474 (2013).
- [17] A. Chernikov, A. M. van der Zande, H. M. Hill, A. F. Rigosi, A. Velauthapillai, J. Hone, and T. F. Heinz, *Phys. Rev. Lett.* **115**, 126802 (2015).
- [18] See Supplemental Material <http://link.aps.org/supplemental/10.1103/PhysRevLett.120.037401> for additional experimental data and transfer matrix calculations, which includes Refs. [19–21].
- [19] P. J. Zomer, M. H. D. Guimares, J. C. Brant, N. Tombros, and B. J. van Wees, *Appl. Phys. Lett.* **105**, 013101 (2014).
- [20] H. Bruus and K. Flensberg, *Many-Body Quantum Theory in Condensed Matter Physics: An Introduction*, Oxford Graduate Texts (Oxford University Press, Oxford, 2004).
- [21] W. Schirmacher, *Theory of Liquids and Other Disordered Media: A Short Introduction*, Lecture Notes in Physics (Springer, New York, 2015).
- [22] A. F. van Loo, A. Fedorov, K. Lalumière, B. C. Sanders, A. Blais, and A. Wallraff, *Science* **342**, 1494 (2013).
- [23] T. Jakubczyk, V. Delmonte, M. Koperski, K. Nogajewski, C. Faugeras, W. Langbein, M. Potemski, and J. Kasprzak, *Nano Lett.* **16**, 5333 (2016).
- [24] D. Krasnozhan, D. Lembke, C. Nyffeler, Y. Leblebici, and A. Kis, *Nano Lett.* **14**, 5905 (2014).
- [25] P. Back, M. Sidler, O. Cotlet, A. Srivastava, N. Takemura, M. Kroner, and A. Imamoglu, *Phys. Rev. Lett.* **118**, 237404 (2017).
- [26] H. Yu, G.-B. Liu, P. Gong, X. Xu, and W. Yao, *Nat. Commun.* **5**, 3876 (2014).
- [27] D. Y. Qiu, T. Cao, and S. G. Louie, *Phys. Rev. Lett.* **115**, 176801 (2015).
- [28] B. Huang, G. Clark, E. Navarro-Moratalla, D. R. Klein, R. Cheng, K. L. Seyler, D. Zhong, E. Schmidgall, M. A. McGuire, D. H. Cobden, W. Yao, D. Xiao, P. Jarillo-Herrero, and X. Xu, *Nature (London)* **546**, 270 (2017).